IEEE Access
Multidisciplinary | Rapid Review | Open Access Journal

Received August 16, 2019, accepted August 28, 2019, date of publication September 12, 2019, date of current version October 4, 2019.

Digital Object Identifier 10.1109/ACCESS.2019.2941044

Comparative Analysis of Input Power Factor Control Techniques in Matrix Converters Based on Model Predictive and Space Vector Control Schemes

ZAHRA MALEKJAMSHIDI[1], (Member, IEEE), MOHAMMAD JAFARI[1], (Senior Member, IEEE), JIANGUO ZHU[2], (Senior Member, IEEE), AND DAN XIAO[3], (Member, IEEE)

[1]School of Electrical and Data Engineering, University of Technology Sydney, Sydney, NSW 2007, Australia
[2]School of Electrical and Information Engineering, The University of Sydney, Sydney, NSW 2006, Australia
[3]School of Electrical Engineering and Telecommunications, University of New South Wales, Sydney, NSW 2052, Australia

Corresponding author: Zahra Malekjamshidi (z_malekjamshidi@ieee.org)

ABSTRACT Model Predictive Control (MPC) with a finite control set and space vector modulation (SVM) are the most common control methods for the matrix converters (MCs). This paper is focused on the input and output currents performance analysis of the matrix converter controlled by SVM and MPC. A closed-loop control of the input current displacement angle is employed in the SVM strategy to provide unity input power factor over a wide range of voltage transfer ratio. For MPC, a discrete-time model of the converter, including the input filter and load, are used to predict the input and output currents for each valid switching state. The MPC, SVM, and power factor controlled SVM (PFC-SVM) methods are analyzed in detail, and their performance in controlling the input power factor, current quality, and transient response are compared through numerical simulations and experimental tests.

INDEX TERMS Matrix converters (MCs), space vector modulation (SVM), model predictive control (MPC), current control, power factor control, harmonic distortion.

I. INTRODUCTION

The matrix converter (MC) compared with the conventional back-to-back converters with dc links has several advantages. It is inherently bidirectional, and a sinusoidal source current with little harmonic components is achievable by using a relatively small *LC* input filter which leads to a compact converter. Also, the direct connection of the load side to the input side of the converter can avoid the using of bulky storage capacitors, which are fault-prone components. However, the MC control becomes more difficult than the conventional converters.

In order to improve the performance of MCs, different modulation techniques have been proposed. Most of the publications consider the pulse width modulation (PWM) or space vector modulation (SVM) for this purpose [1]–[5]. As the modulation techniques are considered as open-loop control strategies, a proper closed-loop control scheme is necessary to achieve the desired variation range for the input or output current and output power. However, it is not possible to reach the unity input power factor (PF) for the whole range of the voltage transfer ratio, and it can be obtained only for the maximum voltage ratio by a well-designed input filter.

The model predictive control (MPC) as another option does not need the linear controllers and modulation techniques, and the behavior of the system variables are predicted based on the system model. The switching state is changed with a sampling period (T_{sp}) based on a quality function which evaluates the predictions so that the variables follow their reference values with good accuracy [6]–[8]. In the case that only a set of feasible switching states are applied, the approach is known as the finite control set MPC (FCS-MPC) [6], [7].

One of the main differences between the MPC and SVM is that the SVM strategy imposes a fixed average switching frequency depending on the sampling period and the

The associate editor coordinating the review of this manuscript and approving it for publication was Bohui Wang.

switching pattern, while in MPC, it is variable, depending on the sampling period and the output to input voltage transfer ratio [9]. Even the cost function definition can affect the average switching frequency [6].

In the case of the MC applications, the MPC has been applied for different control objectives. Due to the importance of input current performance, and direct control of the active and reactive powers in MCs, the MPC has been reported as a feasible solution. It has been used to control the output current achieving a unity PF at the input side [9]–[11]. A direct current control at the source and load sides using MPC with unity PF and enhanced quality of the input source current as the main objective has been presented in [12]. Furthermore, the MPC based methods have been proposed in [11] and [13] to ensure sinusoidal and balanced currents at the source and load sides due to the sensitivity of MCs to unbalanced or distorted grid conditions. A predictive based control has been presented in [14] to improve the efficiency, by reducing the switching losses of MC. The MPC has also been used to mitigate the common-mode voltage in MCs [15], [16]. A simplified MPC method for a MC-fed permanent magnet synchronous machine has been proposed in [17] to reduce the calculation efforts imposed by the conventional MPC.

There are some studies which compare the MPC and SVM or use a combination of them as the control technique. As an example, a combination of MPC and SVM features has been employed in [18] to control a MC in order to add the advantages of working at a fixed switching frequency while maintaining all the characteristics of the MPC. In [19], a comparative assessment of the classical SVM and the MPC for current regulation has been presented. In the MPC, the input current has been controlled, which resulted in the unity input PF; however, there is no control on the input current in the presented SVM method. Therefore, the ability of the unity power factor control of the SVM is limited to the case of maximum voltage transfer ratio.

In contrast, this paper considers the unity input PF control of the SVM for the whole range of the voltage transfer ratio, using a closed-loop control without any impact on the SVM modulation process. This provides a basis for comparison of the performance of the classical SVM and the MPC in controlling the input PF. Therefore, not only the results of the common SVM can be compared with the MPC, as presented in [19], but also with the power factor controlled SVM (PFC-SVM). Different methods have been proposed for controlling the input PF in the SVM method. In [20], a new direct-SVM method for input PF control of MC has been proposed. A closed-loop controlled classical SVM has been used in [21] and [22] to adjust the input PF for torque and flux control of a synchronous machine, and an ac-dc matrix rectifier respectively.

The main contribution of this work is to compare the performance of MPC, SVM, and PFC-SVM strategies in input PF control of the MCs, based on simulations and experimental results. The control settings ensure a similar range of average switching frequency. The control goals are input unity PF at any voltage transfer ratio, as well as regulation of the input and output currents according to their references which are imposed to have a sinusoidal waveform with low harmonic distortion. In the following sections, a general approach on MPC technique which directly controls the states of the MC switches, without any modulator, and the SVM with closed-loop linear controllers will be presented. The main focus will be on the comparison of the control performance in terms of the input PF control, the quality of the input and output currents, and the dynamic response to a step change of the load current. Finally, simulated and experimental verifications for the control methods have been presented and discussed.

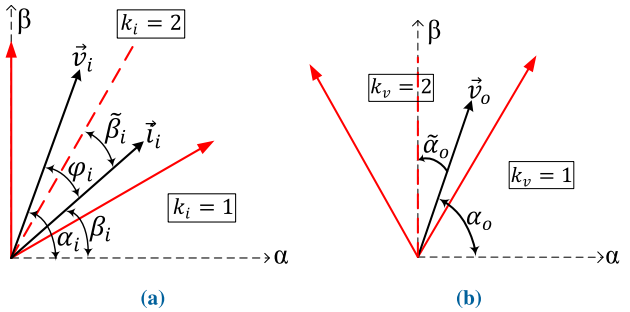

FIGURE 1. a) Input voltage and current vectors in the second sector, b) output reference vector in the second sector.

II. INPUT POWER FACTOR CONTROL USING SVM

The SVM is based on the instantaneous space vectors of the currents and voltages which present three-phase time-variant quantities in a complex plane [23]–[25]. Like the other modulation techniques, SVM determines how the bidirectional switches which are arranged to connect the input phases to the output legs can be switched to generate the sinusoidal input and output currents, and to control the input PF.

The conventional SVM utilizes 21 states (including active and zero vectors) of the 27 safe switching configurations, and does not consider the rotating vectors. The input current and output voltage vectors related to the active switching configurations can be shown in six different directions [2], [3], [26]. Fig. 1 shows the vectors in the second sector of the switching hexagons. The current and voltage space vectors are constructed using a combination of two adjacent vectors in their related sector. As the application time of the switching configurations is variable, a fixed sampling period (T_{sp}) is selected, and a sequence of the switching configurations are applied within the sampling period. The fixed sampling period results in the fixed switching frequency, which depends on the switching pattern, and the number of included zero vectors. Selecting a proper switching pattern can reduce the number of switching instants, and consequently, the switching loss.

In this paper, a double-sided symmetrical switching pattern using one zero vector is applied, and the average switching

frequency of each bidirectional switch is $f_s = \frac{8}{9T_{sp}}$ (the number of state changes of the bidirectional switches per second) [2]–[4]. A fixed switching frequency can improve the input filter size and harmonic performance, and mitigate the switching loss.

Variable '$\bar{x}$' with a bar sign over stands for a vector whose components represent the values of the three-phase system variables. Therefore, the voltages and currents of the input source ($\bar{v}_s, \bar{i}_s$), input ($\bar{v}_i, \bar{i}_i$) and output ($\bar{v}_o, \bar{i}_o$) of the MC can be defined as:

$$\bar{v}_s = \begin{bmatrix} v_{sA} \\ v_{sB} \\ v_{sC} \end{bmatrix}, \quad \bar{v}_i = \begin{bmatrix} v_A \\ v_B \\ v_C \end{bmatrix}, \bar{v}_o = \begin{bmatrix} v_X \\ v_Y \\ v_Z \end{bmatrix} \tag{1}$$

$$\bar{i}_s = \begin{bmatrix} i_{sA} \\ i_{sB} \\ i_{sC} \end{bmatrix}, \quad \bar{i}_i = \begin{bmatrix} i_A \\ i_B \\ i_C \end{bmatrix}, \bar{i}_o = \begin{bmatrix} i_X \\ i_Y \\ i_Z \end{bmatrix} \tag{2}$$

The duty cycles of the switching configurations can be calculated as [27]:

$$d_1 = m\cos(\tilde{\alpha}_o - \frac{\pi}{3})\cos(\tilde{\beta}_i - \frac{\pi}{3}) \tag{3}$$

$$d_2 = m\cos(\tilde{\alpha}_o - \frac{\pi}{3})\cos(\tilde{\beta}_i + \frac{\pi}{3}) \tag{4}$$

$$d_3 = m\cos(\tilde{\alpha}_o + \frac{\pi}{3})\cos(\tilde{\beta}_i - \frac{\pi}{3}) \tag{5}$$

$$d_4 = m\cos(\tilde{\alpha}_o + \frac{\pi}{3})\cos(\tilde{\beta}_i + \frac{\pi}{3}) \tag{6}$$

$$d_0 = 1 - (d_1 + d_2 + d_3 + d_4) \tag{7}$$

$$m = \frac{2q}{\sqrt{3}\cos\varphi_i}, \quad q = \frac{V_o}{V_i}, \tag{8}$$

where q is the voltage transfer ratio, and m the modulation index. $\tilde{\beta}_i$ and $\tilde{\alpha}_o$ are the phase angles of the input current and the output voltage reference vectors, respectively, referred to the bisecting line of the corresponding sector ($-\frac{\pi}{6} < \tilde{\alpha}_o < +\frac{\pi}{6}, -\frac{\pi}{6} < \tilde{\beta}_i < +\frac{\pi}{6}$), as illustrated in Fig. 1.

As mentioned before, the SVM is an open-loop control, and as shown in Fig. 2a, the closed-loop control based on the voltage oriented control (VOC) strategy is utilized to control the output current [28], [29]. The output currents are transformed into their equivalent direct-quadrature (d-q) synchronous reference frame and are compared to the reference values to determine the errors. The resultant errors then are processed by the decoupled proportional-integral (PI) controllers to generate the reference load voltages ($\bar{v}_o^r$), which are finally transferred to the modulation process to obtain the switching signals. In the proposed VOC method, the PI controllers are used to generate the three-phase output reference voltage $\bar{v}_o^r$. In the purpose of unity input PF, the d-q elements of the output reference current are selected as, $i_{o(d)}^r = I_o^r$ and $i_{o(q)}^r = 0$, where I_o^r is the amplitude of the output reference current. Also, v_{oa}, v_{ob}, v_{oc} are the initial output reference voltages which determine the output frequency (ω_o) and the angle δ for the closed-loop control of the output current as shown in Fig. 2b.

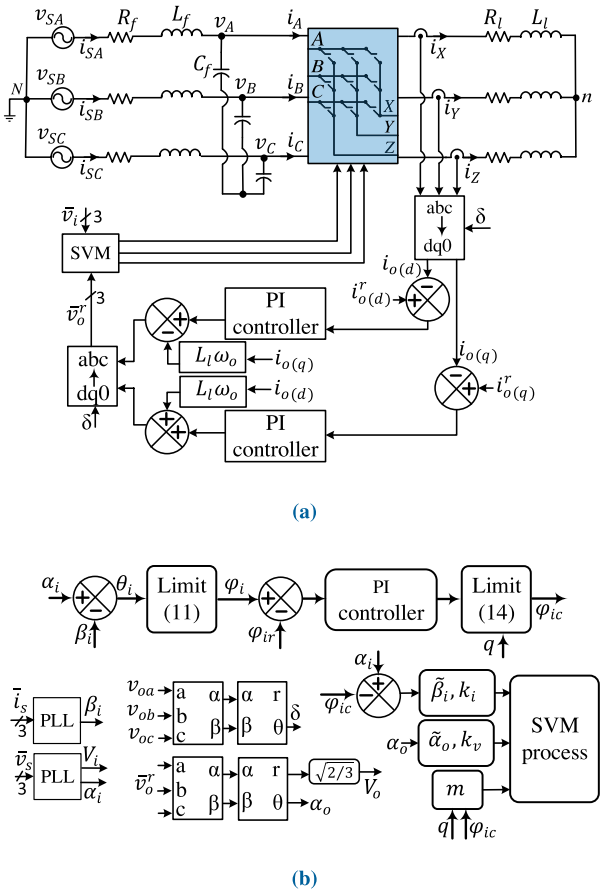

FIGURE 2. DMC scheme, a) SVM strategy, with closed-loop control of the output current, b) Closed-loop control of the input power factor in the PFC-SVM strategy.

III. INPUT FILTER DESIGN AND CLOSED-LOOP CONTROL OF THE INPUT DISPLACEMENT ANGLE

To reduce the reactive power, the input filter needs to be designed properly, as the input PF is affected by the input filter parameters. In the SVM, displacement angle φ_i between the filtered input current to the source ($\bar{i}_s$) and the source voltage ($\bar{v}_s$) depends on the voltage transfer ratio q. Zero displacement angle (unity PF) is achievable for the maximum voltage ratio $q = 0.866$, and the filter designation is according to this assumption. On the other hand, the minimum input PF, which happens at the minimum output power $P_{o,min}$ (10% of rated input active power $P_{i,n}$) should be taken into account. In this paper, considering $PF_{min} = 0.8$, the input filter capacitance has been defined as [30]:

$$\begin{aligned} C_f &\le \frac{0.1P_{i,n}\tan(\varphi_{i,max})}{3\omega_i V_{i,n}^2} \\ P_{i,n} &= 3V_{i,n}I_{i,n} \\ PF_{min} &= cos(\varphi_{i,max}) = 0.8 \end{aligned} \tag{9}$$

where $V_{i,n}$ and $I_{i,n}$ are the *rms* values of the rated input phase voltage and current of the MC, and ω_i is the supply angular frequency. To determine L_f, it should be considered that the

voltage drop across the input filter inductance at the rated input current should be minimized so that $v_{si} \approx v_i$, and can be selected by using the cut-off frequency $f_c = \frac{1}{2\pi\sqrt{L_f C_f}}$. f_c should be considered more than twenty times of the input frequency f_i and less than one-third of the switching frequency of a bidirectional switch [31].

After selecting the proper input filter parameters, the phase shift imposed by the filter components for the output powers less than the rated power can be modified by a closed-loop control as illustrated in Fig. 2b [21], [22]. The PFC-SVM strategy relies on the measurement of the instantaneous source voltage and current for calculating the input displacement angle (φ_i). Assuming that:

$$\theta_i = \alpha_i - \beta_i \tag{10}$$

φ_i must be limited between $-\frac{\pi}{2}$ and $\frac{\pi}{2}$ (inductive to capacitive range respectively) as the following:

$$\varphi_i = \begin{cases} \theta_i + 2\pi & if\ (-2\pi \le \theta_i < -\frac{\pi}{2}) \\ \theta_i & if\ (-\frac{\pi}{2} \le \theta_i \le \frac{\pi}{2}) \\ \theta_i - 2\pi & if\ (\frac{\pi}{2} < \theta_i < 2\pi) \end{cases} \tag{11}$$

As mentioned before, the input displacement angle increases when the voltage transfer ratio q reduces, and thus:

$$q \le \frac{\sqrt{3}}{2}\cos\varphi_i \ \Rightarrow\ \varphi_i \ge \left|\cos^{-1}\left(\frac{2q}{\sqrt{3}}\right)\right| \tag{12}$$

Therefore, the limit of the displacement angle can be obtained as:

$$\varphi_{i,lim} = \cos^{-1}\left(\frac{2q}{\sqrt{3}}\right) \tag{13}$$

Considering that $0 < q < \frac{\sqrt{3}}{2}$, the compensated input displacement angle φ_{ic} can then be defined as the following:

$$\varphi_{ic} = \begin{cases} \varphi_i & if\ (-\varphi_{i,lim} < \varphi_i < \varphi_{i,lim}) \\ -\varphi_{i,lim} & if\ (\varphi_i < -\varphi_{i,lim}) \\ \varphi_{i,lim} & if\ (\varphi_i > \varphi_{i,lim}) \end{cases} \tag{14}$$

and if $q > \frac{\sqrt{3}}{2}$, $\varphi_{ic} = 0$. The desired input displacement angle (φ_{ir}), can be achieved by properly tuning of the PI coefficients. To obtain the unity input PF for the whole range of q, the reference input displacement angle should be $\varphi_{ir} = 0$. The compensated input displacement angle φ_{ic} is used in the modulation process, as illustrated in Fig. 2b.

Without the input PF closed-loop control, the assumption $\varphi_i = 0$ in the modulation index m results a unity input PF for the maximum voltage transfer ratio only, not for the whole range of q. It means $\beta_i = \alpha_i$, and therefore, in the calculation related to the input current sector (k_i), the input voltage angle α_i could be used instead of β_i. In the PFC-SVM strategy, φ_{ic} is used in the calculation of m, and α_i–φ_{ic} is applied to determine k_i (referring to Fig. 2b). φ_{ic} is variable and depends on the displacement angle φ_{ir}, the voltage transfer ratio (q), and the passive components of the circuit, especially the input filter components.

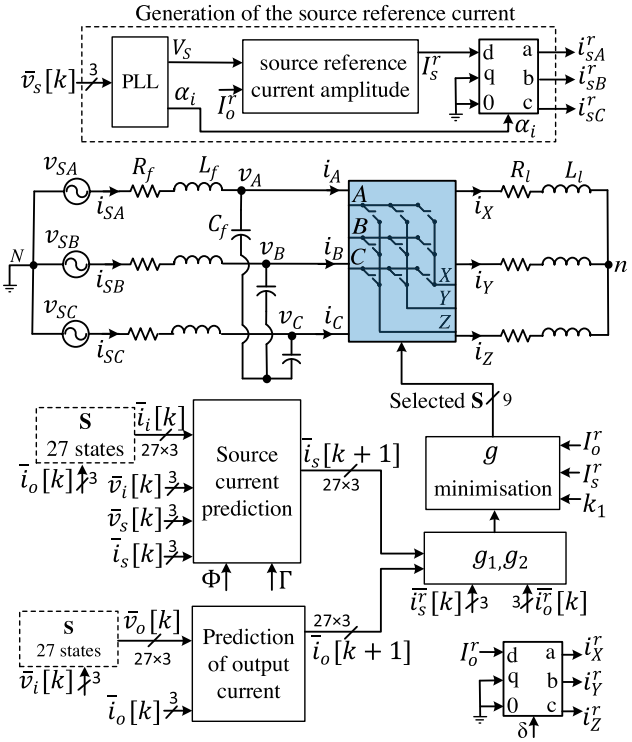

FIGURE 3. Schematic of the MPC for controlling the input and output currents of the DMC.

IV. INPUT POWER FACTOR CONTROL USING MPC

In this section, the MPC strategy is investigated to control the output current of the DMC, and at the same time, the input source current, to obtain a low-distortion current with unity PF. Compared to the SVM strategy, the MPC with a finite control set (FCS-MPC) is a different approach that can effectively control the input and output variables of the MCs. In this method, several system variables can be controlled with a single control function, using appropriate weighting factors. Unlike the common SVM method that does not consider the rotating vectors, the MPC allows the use of all valid switching states.

The power and control circuits of the MC using MPC are shown in Fig. 3. Using the mathematical model of the converter, the values of the system variables for the next sampling period are predicted. A predictive cost function then selects the switching state, which causes the load current to follow its reference waveform with good quality while meeting the other demands [6], [7].

Using the mathematical model of the system, the behavior of the system can be predicted, and the best possible switching state of the converter can then be selected to generate the reference values. The continuous-time model of the system at the load side can be derived as a basis for predicting the output currents as the following:

$$L_l \frac{d\bar{i}_o(t)}{dt} = \bar{v}_o(t) - R_l \bar{i}_o(t) \tag{15}$$

where L_l and R_l are the load inductance and resistance, respectively. In order to realize an accurate computation

within a digital system, the discrete-time model of the output is formed using forward Euler approximation as [10], [19]:

$$\bar{i}_o[k+1] = \frac{T_{sp}}{L_l}\bar{v}_o[k] + \left(1 - \frac{R_l T_{sp}}{L_l}\right)\bar{i}_o[k] \tag{16}$$

where $\bar{i}_o[k+1]$ is the predicted value of the load current, and the output voltage vector $\bar{v}_o[k] = S.\bar{v}_i[k]$ is the dependent variable of the switching states and the input voltage vector, that is calculated for each of the 27 valid switching states. Matrix S shows the switching state of the MC as a function of the switches (S_{kj}), and is represented as follows:

$$S = \begin{bmatrix} S_{XA} & S_{XB} & S_{XC} \\ S_{YA} & S_{YB} & S_{YC} \\ S_{ZA} & S_{ZB} & S_{ZC} \end{bmatrix} \tag{17}$$

and

$$S_{kj} = \begin{cases} 0 & if\ (S_{kj}\ is\ blocking) \\ 1 & if\ (S_{kj}\ is\ conducting) \end{cases} \tag{18}$$

where $k = [X, Y, Z]$ and $j = [A, B, C]$. The modeling equations at the input side of the MC can be developed as:

$$\begin{bmatrix} \frac{d\bar{v}_i(t)}{dt} \\ \frac{d\bar{i}_s(t)}{dt} \end{bmatrix} = A_c \begin{bmatrix} \bar{v}_i(t) \\ \bar{i}_s(t) \end{bmatrix} + B_c \begin{bmatrix} \bar{v}_s(t) \\ \bar{i}_i(t) \end{bmatrix} \tag{19}$$

where the matrix coefficients are:

$$A_c = \begin{bmatrix} 0 & \frac{1}{C_f} \\ -\frac{1}{L_f} & -\frac{R_f}{L_f} \end{bmatrix}, \quad B_c = \begin{bmatrix} 0 & -\frac{1}{C_f} \\ \frac{1}{L_f} & 0 \end{bmatrix} \tag{20}$$

In analogy to the output, the corresponding discrete-time model of the input side can be determined as [10], [16]:

$$\begin{bmatrix} \bar{v}_i[k+1] \\ \bar{i}_s[k+1] \end{bmatrix} = A_q \begin{bmatrix} \bar{v}_i[k] \\ \bar{i}_s[k] \end{bmatrix} + B_q \begin{bmatrix} \bar{v}_s[k] \\ \bar{i}_i[k] \end{bmatrix} \tag{21}$$

$$A_q = e^{A_c T_{sp}}, \quad B_q = \int_0^{T_{sp}} e^{A_c(T_{sp}-\tau)} B_c d\tau \tag{22}$$

Therefore, the input source current predictive equations are defined as:

$$\bar{i}_s[k+1] = A_q(2,1)\bar{v}_i[k] + A_q(2,2)\bar{i}_s[k] + B_q(2,1)\bar{v}_s[k] + B_q(2,2)\bar{i}_i[k] \tag{23}$$

where $\bar{i}_i[k]$ is obtained from $\bar{i}_o[k]$ for all the valid switching states. The amplitude of the source reference current (I_s^r) can be determined as a function of the efficiency η from [12]:

$$I_s^r = \frac{V_s\lambda + \sqrt{V_s^2\lambda^2 + 4\lambda R_f R_l I_o^{r\,2}/\eta}}{2R_f\lambda}$$
$$\lambda = 8\pi^2 f_i^2 L_f C_f - 1 \tag{24}$$

For instance, the first phase of the source reference current can be defined as:

$$i_{sA}^r(t) = I_s^r \cos(\omega_i t - \varphi_{ir}) \tag{25}$$

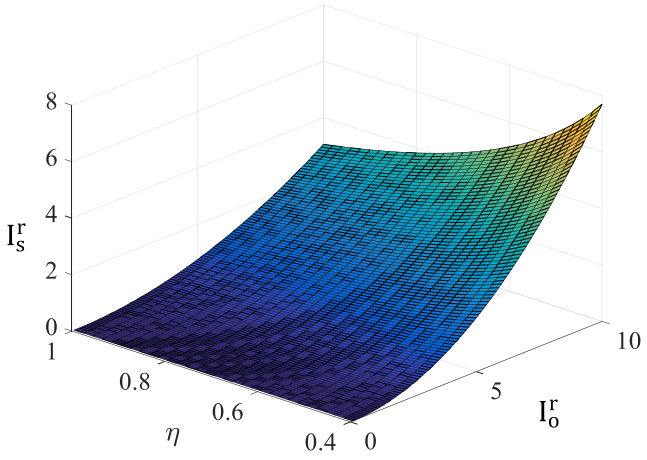

FIGURE 4. Input source current amplitude against the output current amplitude and system efficiency.

where φ_{ir} is the reference displacement angle, and is equal to zero for unity input PF. To generate the three-phase $i_s^r(t)$, the source voltage angle and amplitude should be obtained through a three-phase phase-locked loop (PLL), as shown in Fig. 3. Variations of the input source current amplitude (I_s^r) against the amplitude of the output current (I_o^r), and the converter efficiency (η) are shown in Fig. 4. The graph is plotted for the system parameters in Table 1, with the input source voltage 400 V line to line.

The cost function evaluates the predicted input and output currents for all valid switching states according to the control goals. In this paper, the main goals are operation at the unity PF with a good quality of the current on the input side, and the current control on the output side of the converter. As shown in Fig. 3, the generated input and output reference currents are as below:

$$\bar{i}_s^r = \begin{bmatrix} i_{sA}^r \\ i_{sB}^r \\ i_{sC}^r \end{bmatrix}, \quad \bar{i}_o^r = \begin{bmatrix} i_X^r \\ i_Y^r \\ i_Z^r \end{bmatrix} \tag{26}$$

Therefore, the cost function for the regulation of the output current can be defined as:

$$g_1 = \left(i_X^r[k] - i_X[k+1]\right)^2 + \left(i_Y^r[k] - i_Y[k+1]\right)^2 + \left(i_Z^r[k] - i_Z[k+1]\right)^2 \tag{27}$$

and at the source side as:

$$g_2 = \left(i_{sA}^r[k] - i_{sA}[k+1]\right)^2 + \left(i_{sB}^r[k] - i_{sB}[k+1]\right)^2 + \left(i_{sC}^r[k] - i_{sC}[k+1]\right)^2 \tag{28}$$

This strategy leads to the direct control of the input and output currents at the same time, while both currents are sinusoidal with good quality. Furthermore, the input displacement angle remains zero for any output current amplitude [12]. The final cost function used for the minimization algorithm

TABLE 1. Simulation and experimental setup parameters.

Source voltage (phase to phase)	$140\ Vrms$
Input frequency	$f_i = 50Hz$
Output frequency	$f_o = 60Hz$
Input filter inductance	$L_f = 3mH$
Input filter capacitance[1]	$C_f = 6.6\mu F$
Input filter resistance	$R_f = 0.5\Omega$
Load inductance	$L_l = 6mH$
Load resistance	$R_l = 10\Omega$
Damping resistance	$R_d = 20\Omega$
Sampling time (SVM)	$T_{sp} = 100\mu s$
Sampling time (MPC)	$T_{sp} = 24\mu s$
Weighting factor for $I_o^r = 8\ A$	$k_1 = 10$
Weighting factor for $I_o^r = 4\ A$	$k_1 = 1$
Efficiency (simulation)	$\eta = 1$
Efficiency (experimental)	$\eta = 0.8$

[1](Delta connection)

consists the normalized cost functions as the following [19]:

$$g = \frac{g_1}{I_o^{r2}} + k_1 \frac{g_2}{I_s^{r2}} \tag{29}$$

where k_1 is a weighting factor. Finally, the switching state associated with the prediction which generates the minimum cost function is chosen for the following time interval.

V. NUMERICAL SIMULATIONS

To compare the operation of the SVM, the PFC-SVM, and the proposed MPC for input PF control, numerical simulation of a DMC is carried out for the control techniques using PSIM software. The system parameters have been selected to match the experimentally developed prototype, as shown in Table 1. The selected sampling times (T_{sp}) for SVM and MPC are different to achieve an almost equal average switching frequency (f_s) for a fair comparison. Different values of the sampling times were tested in the simulation, and the number of switching instants per second, counted by the incremental counters, were compared to select the proper switching frequency for each control method. Unlike the SVM, in the MPC, the average switching frequency f_s is variable as the cost function can select a switching state as the optimal one for more than one switching period. The average switching frequency depends on some parameters like sampling period, modulation index [9], weighting factor [32], and cost function [6]. It decreases as the voltage transfer ratio increases, although the minimum switching frequency can be obtained for $m = 1$ [9].

In order to suppress the resonance of the input filter, different damping methods have been proposed in the literature [8], [33], [34]. In this paper,three 20Ω damping resistors have been connected in parallel to the filter inductors to assure its normal stable operation. The small currents of the damping resistors do not cause high power dissipation. Although for the higher input currents, smaller values of the damping resistors are needed to guarantee the system stability. The power loss cannot be ignored in this case, and active damping methods are preferred.

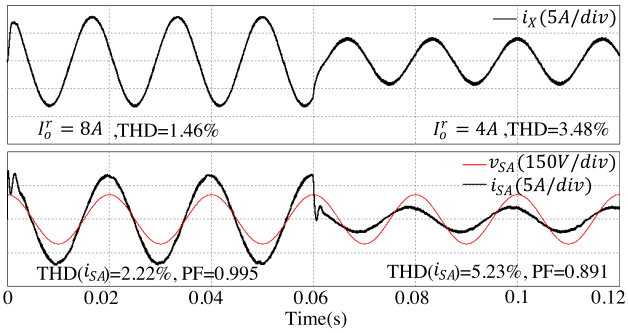

FIGURE 5. Simulated closed-loop output current control using the SVM with a step change in the load current amplitude, without PF control.

Figs. 5 to 7 show the simulated results of the DMC using SVM and MPC control methods, where the reference output current amplitude (I_o^r) is kept constant at 8 A for 0.06s, and then steps down to 4 A. The step change is applied to show the behavior of the control methods in two different voltage transfer ratios, and also the dynamic behavior of the system. The transient time, THDs of the input and output currents, and the input PF are the parameters for comparison.

Fig. 5 presents the waveforms of the input phase voltage and current, and the output current of the SVM method with only the closed-loop output current control. It is evident that the input current at first is in phase with the source current, but in the second half, it is leading by 27° with respect to the source voltage. This completely agreed with the feature of the input PF in SVM that is dependent on the voltage transfer ratio, and the reduction in the load current leads to the shift of the input current. In fact, at the step change instant when a change in the load current occurs, the displacement angle of the input current happens immediately, which shows the fast response of the SVM and the PI controller. In addition to the input PF, THDs of the currents are smaller for the higher voltage ratio. When $I_o^r = 8A$, the THDs of the input and output currents are 2.22% and 1.46%, while for $I_o^r = 4A$ they increase to 5.23% and 3.48%, respectively.

In Fig. 6, in addition to the closed-loop control of the output current, the PF closed-loop strategy has been employed to adjust the input current displacement angle to zero. The mentioned input PF in the figure verifies the performance of the PFC-SVM strategy for input displacement angle control. The measured input PF is very close to unity before and after the step-change. However, the input current THD in the first 0.06s is considerably higher than that of SVM without PF control, there is not a significant difference for other waveforms, which can be related to the parameters of the PI controllers. Overall, the transient response to the current step and the unity PF control is fast, with negligible overshoot.

The input and output currents with their THDs and the resultant input PF for the MPC method are shown in Fig. 7.

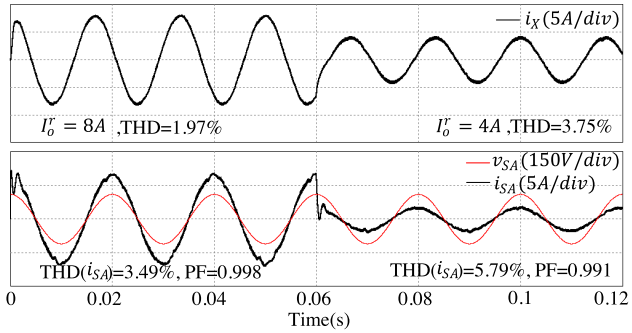

FIGURE 6. Simulated output current control using the PFC-SVM with a step change in the load current amplitude.

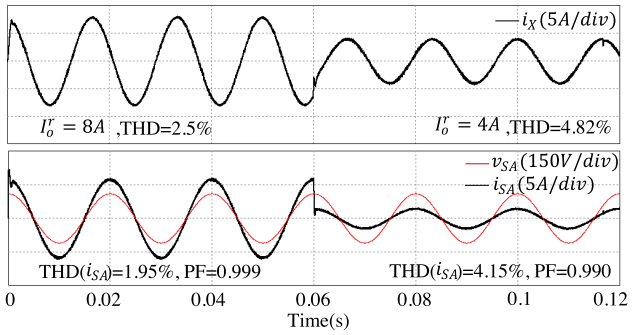

FIGURE 7. Simulated output current control using the MPC with a step change in the load current.

Two different values of the weighting factor have been applied for the output current levels as illustrated in Table 1. The selection process is based on a trade-off between the source current and load current qualities, and can be selected by trial and error procedure. Some guidelines have been provided in [32], which can be helpful for this process. As can be seen, the reference input displacement angle $\varphi_i = 0$ has been kept constant in both current values without any dependency on the voltage ratio. The THDs of the input and output currents are 1.95% and 2.5% respectively, for the output current amplitude $I_o^r = 8A$. Similar to the SVM, there is a considerable increase in the THDs when the output reference current amplitude is decreased to 4A. The THD rises to 4.15% and 4.82% for the input and output currents respectively. The simulation results for all cases are presented in Table 2 for easier comparison. It is worthwhile to mention that the comparison results of the simulation and experimental tests of the SVM and the MPC are consistent with the results obtained in [19].

The number of switching instants per second is registered using nine incremental counters, which are triggered by any state changing of the switches within 0.1 s of the simulation test. The measured values of average, minimum, and maximum switching frequency of the bidirectional switches in the control methods have been illustrated in Table 2 for two cases of the output currents, and three different control techniques.

The expected amount of average switching frequency $f_s(ave)$ for SVM is $\frac{8}{9T_{sp}} = 8890\ Hz$ [2]–[4]. As can be seen,

TABLE 2. Simulation measurements for SVM and MPC methods.

Output reference current amplitude	Measured parameters	SVM	PFC-SVM	MPC
$I_o^r = 8A$	THD (i_s)	2.22%	3.49%	1.95%
	THD (i_o)	1.46%	1.97%	2.5%
	Input PF	0.995	0.998	0.999
	f_s (ave)	8950	9800	9890
	f_s (min)	8830	9600	9490
	f_s (max)	9020	9970	10170
$I_o^r = 4A$	THD (i_s)	5.23%	5.79%	4.15%
	THD (i_o)	3.48%	3.75%	4.82%
	Input PF	0.891	0.991	0.990
	f_s (ave)	8910	10200	9730
	f_s (min)	8830	10110	9200
	f_s (max)	8950	10310	9970

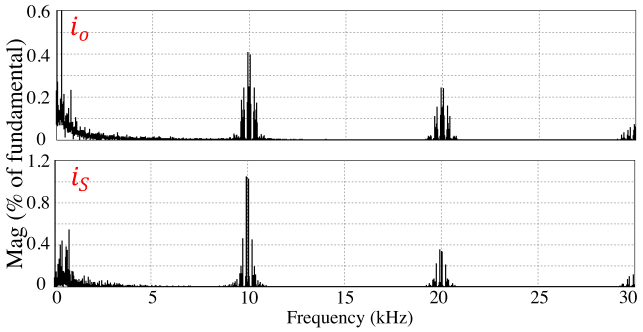

FIGURE 8. Simulation results of the output and input currents spectrum expressed as a percentage of fundamental amplitude for the SVM when $I_o^r = 8A$.

in SVM method without the PF control, the measured $f_s(ave)$ is about 8950 Hz and 8910 Hz for the output currents 8A and 4A respectively, which are in the range of the expected average switching frequency. These amounts arise to 9800 Hz and 10200Hz by adding the closed-loop control of the input PF, which means the input PF compensation in the PFC-SVM leads to an increase in the switching number. This incremental trend is also seen in the MPC strategy that inherently includes the PF compensation, which in fact, has the average switching frequency close to the PFC-SVM. The minimum switching frequency of a bidirectional switch occurs in the SVM with no PF control ($f_s(min) = 8830\ Hz$), and the maximum one in the PFC-SVM ($f_s(max) = 10310\ Hz$). Figs. 8 and 9 present the spectra of the output and input currents, expressed as a percentage of fundamental amplitude, for the SVM and MPC algorithms when $I_o^r = 8A$. As can be seen in Fig. 8, in the SVM method, the harmonics are in the range of switching frequency (f_s) and its multiples, which confirms fixed switching-frequency operation. On the other hand, Fig. 9 reveals that the MPC does not lead to a fixed switching frequency.

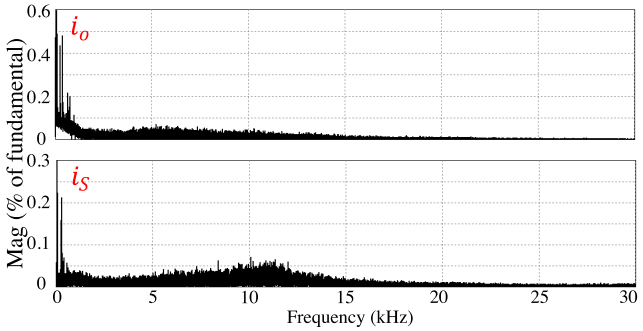

FIGURE 9. Simulation results of the output and input currents spectrum expressed as a percentage of fundamental amplitude for the MPC when $I_o' = 8A$.

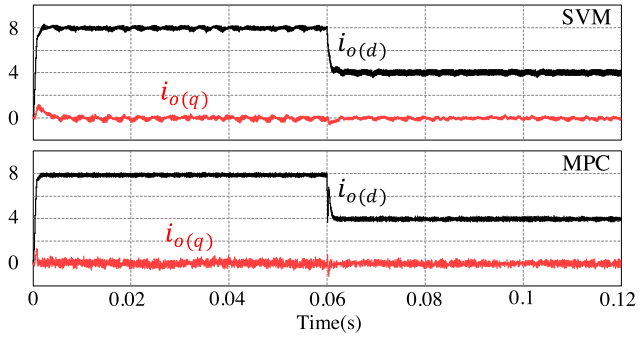

FIGURE 10. Simulation results of the *d* and *q* parts of the load current during a step change in the amplitude.

The transient response to the reference change is an important aspect for the control strategies which is evaluated by comparing the $d-q$ parts of the output current ($i_{o(d)}$ and $i_{o(q)}$) in Fig. 10. As can be seen, both SVM and MPC behave comparably under this situation.

As the MPC is inherently dependent on the model parameters, the utilization of a model of the load is necessary to predict the future behaviour of the output current. To evaluate the effect of change in the load parameters, four simulation tests have been done by doubling or halving the load parameters. After adjusting the MPC parameters based on the original load parameters ($R_l = 10\Omega$, and $L_l = 3mH$), doubling the load inductance ($L_l = 6mH$) improved the THD of the output current, while halving it ($L_l = 1.5mH$), increased it. In both cases, the output current followed the reference properly without considerable effect on PF and THD of the input current. However, applying the same changes to the load resistance resulted an un-regulated output current, with no considerable effect on the THD. By reducing the load resistance and as a result reducing the voltage transfer ratio, the THD of the input current increased, and vice versa. As the impedance of the load inductor is much less than the load resistance, the effect of the inductance change is not considerable compared to the resistance.

VI. EXPERIMENTAL RESULTS

To validate the theory and numerical simulation results, a prototype of a DMC was designed, implemented, and

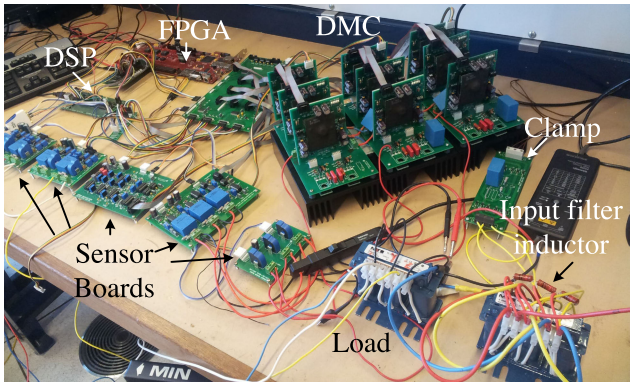

FIGURE 11. Experimental setup of the DMC prototype.

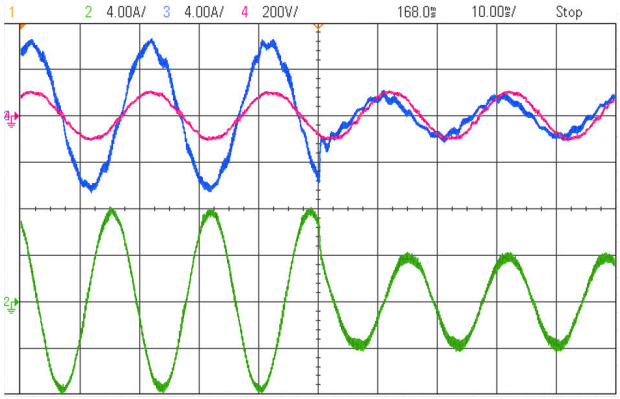

FIGURE 12. Experimental results of the closed-loop output current control using SVM, with a step change in the load current without PF control.

tested experimentally, as shown in Fig. 11. The converter consists of an arrangement of 18 IGBTs (IRG7PH42UD1-EP) containing an antiparallel connected diode, in the common-collector bidirectional configuration. The driving signals are generated by two channels hybrid integrated driver circuits (VLA567-01R) with built-in short circuit protection circuits. The LEM sensors, LTSR 25-NP and LV 25-P, have been used to measure the currents and voltages. The control schemes have been implemented in C code by using a digital signal processor (DSP) model TMS320F28335, and the control of the current commutation is provided by a field programmable gate array (FPGA) processor of a Xilinx spartan6LX150T development board which follows a current-based four-step commutation process. A DSOX2004A KEYSIGHT oscilloscope is utilized to record the waveforms.

The proposed modulation and control algorithms have been tested on the experimental prototype, which the RL load, input source voltage, and input filter parameters have been selected the same as the numerical simulations. The control conditions and factors are also chosen as presented in Table 1. Figs. 12 to 14 are experimental waveforms showing the results for the control methods.

Fig. 12 shows the waveforms of the input line current and phase voltage, and the output phase current of the three-phase DMC. The SVM method with the closed-loop output current control is employed, and no direct control was applied

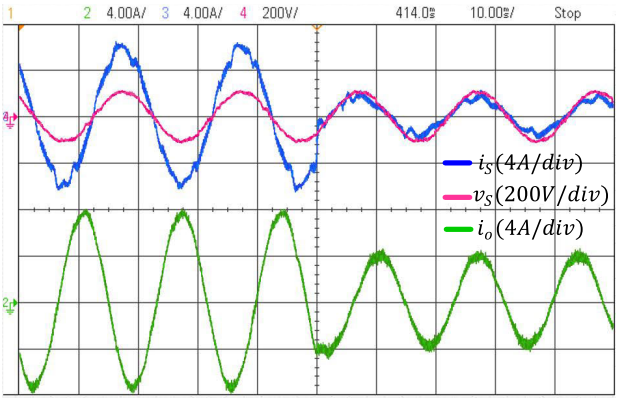

FIGURE 13. Experimental results of the PFC-SVM strategy, with a step change in the load current.

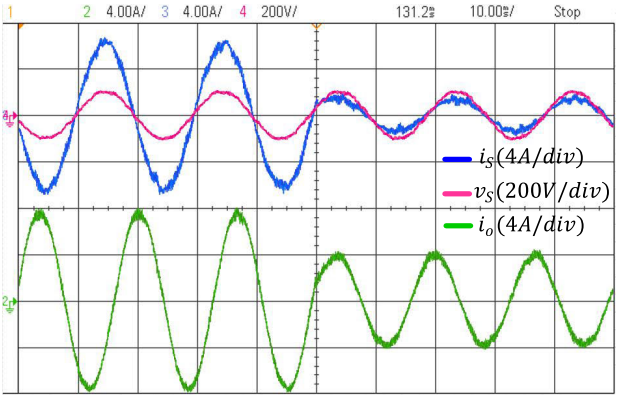

FIGURE 14. Experimental results of the output current control using MPC, with a step change in the load current.

to the input current phase angle. As can be seen, when the output current steps down to $4A$, the input current PF changes by about 0.128, which means a change of the displacement angle around 22.35°. Fig. 13 experimentally verifies that the PFC-SVM strategy is capable of the direct control of the input current phase angle. It shows the resultant waveforms with the same operating conditions in Fig. 12, in addition to using the closed-loop PI controller of the input PF. The zero input current displacement kept almost unchanged after the step-down change of the output current. Also, the source current and voltage resulted from the MPC strategy in Fig. 14, are in phase for both output reference current values. Table 3 presents the results of the experimental tests. Considering the THDs of the input and output currents, using the selected control factors, MPC offers a lower THD of the input source current, although the THD of the output current is slightly larger than the SVM method. The harmonic distortions of the input source current and load current for the PFC-SVM and the MPC can be observed in detail in Figs. 15 and 16. The experimental results agree with the simulation results comparing to the waveforms in section V.

VII. COMPARISON OF THE RESULTS

In all presented strategies, it can be seen that the control goal of the input and output currents regulation are met with proper reference tracking and dynamic responses.

TABLE 3. Experimental measurements for SVM and MPC methods.

Output reference current amplitude	Measured parameters	SVM	PFC-SVM	MPC
$I_o^r = 8A$	THD (i_s)	9.45%	11.57%	5.38%
	THD (i_o)	3.23%	3.83%	4.51%
	Input PF	0.990	0.999	0.999
$I_o^r = 4A$	THD (i_s)	15.63%	17.78%	9.24%
	THD (i_o)	5.76%	5.6%	5.92%
	Input PF	0.862	0.991	0.992

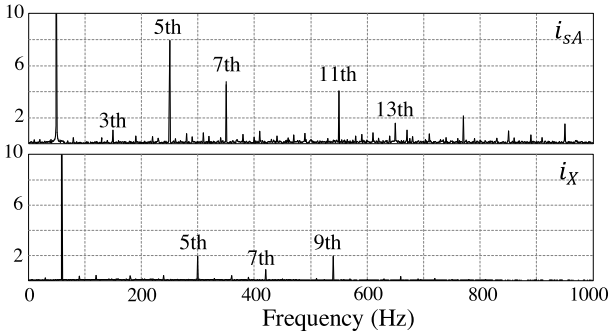

FIGURE 15. Experimental results of the spectrum PFC-SVM.

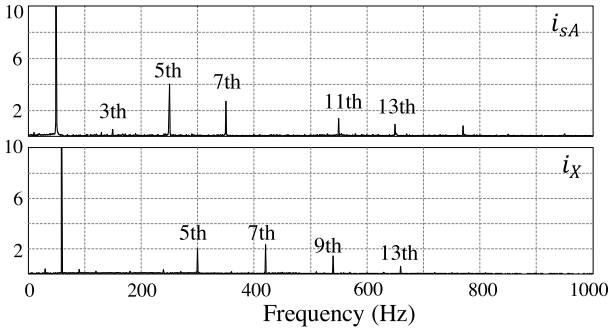

FIGURE 16. Experimental results of the spectrum MPC.

Although the comprehension and implementation of the MPC is simple compared to the SVM strategy, it is significantly dependent on the system parameters. Furthermore, in the SVM, the parameters of the PI controllers, and in the MPC, the weighting factors need to be selected using some guidelines [32].

Comparison of the input PF results of the PFC-SVM and the MPC in both numerical simulation and experimental tests indicate very close results. The input PF in both methods is more than 0.99 for the presented output reference currents. Also, the THD measurements show that the SVM method generates input currents that are more distorted than those from the MPC. This result is more visible in the experimental tests. In the case of the THD of the load current, the SVM presents slightly lower values, especially for higher voltage transfer ratio. Furthermore, the dynamic response of the controllers to the current level changes are very similar.

Therefore, in order to achieve unity PF control of a MC, for applications with frequent varying load currents, both methods present acceptable operation.

The proposed MPC and the PFC-SVM can achieve good input and output current performance with input PF close to unity for different levels of the voltage transfer ratios. In the experimental tests, MPC presented a better harmonic quality in the source current than PF-controlled SVM.

VIII. CONCLUSION

Three different MC control strategies, including MPC, SVM, and PFC-SVM, regarding the input and output current quality, and input PF control, were analyzed and compared. Considering numerical simulation and experimental test results, it was seen that the unity power factor control is achievable over a wide range of the voltage transfer ratio in both MPC and PFC-SVM methods. Although, the flexibility of the MPC in the inclusion of the other control factors, and simultaneous control of the input and output currents is a big advantage. All three methods presented a fast transient response of the input PF control to the step change of the output current, however, the resultant distortion of the input current in the MPC was less than the SVM methods. As the goal of the paper was the comparison of the classic SVM and the MPC, the proposed closed-loop PF control was applied without any manipulation of the SVM modulation process. However, as future work, the input PF can be controlled using the new SVM algorithms, which impacts the modulation process directly.

REFERENCES

[1] J. Rodríguez, M. Rivera, J. W. Kolar, and P. W. Wheeler, "A review of control and modulation methods for matrix converters," *IEEE Trans. Ind. Electron.*, vol. 59, no. 1, pp. 58–70, Jan. 2012.

[2] D. Casadei, G. Serra, A. Tani, and L. Zarri, "Optimal use of zero vectors for minimizing the output current distortion in matrix converters," *IEEE Trans. Ind. Electron.*, vol. 56, no. 2, pp. 326–336, Feb. 2009.

[3] P. Nielsen, F. Blaabjerg, and J. K. Pedersen, "Space vector modulated matrix converter with minimized number of switchings and a feedforward compensation of input voltage unbalance," in *Proc. Int. Conf. Power Electron., Drives Energy Syst. Ind. Growth*, vol. 2, Jan. 1996, pp. 833–839.

[4] K. B. Larsen, A. H. Jorgensen, L. Helle, and F. Blaabjerg, "Analysis of symmetrical pulse width modulation strategies for matrix converters," in *Proc. IEEE 33rd Annu. IEEE Power Electron. Spec. Conf.*, vol. 2, Jun. 2002, pp. 899–904.

[5] A. Alesina and M. Venturini, "Analysis and design of optimum-amplitude nine-switch direct AC-AC converters," *IEEE Trans. Power Electron.*, vol. 4, no. 1, pp. 101–112, Jan. 1989.

[6] S. Kouro, P. Cortes, R. Vargas, U. Ammann, and J. Rodriguez, "Model predictive control—A simple and powerful method to control power converters," *IEEE Trans. Ind. Electron.*, vol. 56, no. 6, pp. 1826–1838, Jun. 2009.

[7] P. Cortés, M. P. Kazmierkowski, R. M. Kennel, D. E. Quevedo, and J. Rodríguez, "Predictive control in power electronics and drives," *IEEE Trans. Ind. Electron.*, vol. 55, no. 12, pp. 4312–4324, Dec. 2008.

[8] M. Rivera, C. Rojas, J. Rodríguez, P. Wheeler, B. Wu, and J. R. Espinoza, "Predictive current control with input filter resonance mitigation for a direct matrix converter," *IEEE Trans. Power Electron.*, vol. 26, no. 10, pp. 2794–2803, Oct. 2011.

[9] S. Müller, U. Ammann, and S. Rees, "New time-discrete modulation scheme for matrix converters," *IEEE Trans. Ind. Electron.*, vol. 52, no. 6, pp. 1607–1615, Dec. 2005.

[10] R. Vargas, J. Rodríguez, U. Ammann, and P. W. Wheeler, "Predictive current control of an induction machine fed by a matrix converter with reactive power control," *IEEE Trans. Ind. Electron.*, vol. 55, no. 12, pp. 4362–4371, Dec. 2008.

[11] M. Rivera, J. Rodríguez, J. R. Espinoza, and H. Abu-Rub, "Instantaneous reactive power minimization and current control for an indirect matrix converter under a distorted AC supply," *IEEE Trans. Ind. Informat.*, vol. 8, no. 3, pp. 482–490, Aug. 2012.

[12] M. Rivera, J. Rodriguez, J. R. Espinoza, T. Friedli, J. W. Kolar, A. Wilson, and C. A. Rojas, "Imposed sinusoidal source and load currents for an indirect matrix converter," *IEEE Trans. Ind. Electron.*, vol. 59, no. 9, pp. 3427–3435, Sep. 2012.

[13] W. Xiong, Y. Sun, J. Lin, M. Su, H. Dan, M. Rivera, and J. M. Guerrero, "A cost-effective and low-complexity predictive control for matrix converters under unbalanced grid voltage conditions," *IEEE Access*, vol. 7, pp. 43895–43905, 2019.

[14] R. Vargas, U. Ammann, and J. RodrÍguez, "Predictive approach to increase efficiency and reduce switching losses on matrix converters," *IEEE Trans. Power Electron.*, vol. 24, no. 4, pp. 894–902, Apr. 2009.

[15] R. Vargas, U. Ammann, J. Rodriguez, and J. Pontt, "Predictive strategy to control common-mode voltage in loads fed by matrix converters," *IEEE Trans. Ind. Electron.*, vol. 55, no. 12, pp. 4372–4380, Dec. 2008.

[16] R. Vargas, J. Rodriguez, C. A. Rojas, and M. Rivera, "Predictive control of an induction machine fed by a matrix converter with increased efficiency and reduced common-mode voltage," *IEEE Trans. Energy Convers.*, vol. 29, no. 2, pp. 473–485, Jun. 2014.

[17] M. Siami, D. A. Khaburi, and J. Rodriguez, "Simplified finite control set-model predictive control for matrix converter-fed PMSM drives," *IEEE Trans. Power. Electron.*, vol. 33, no. 3, pp. 2438–2446, Mar. 2018.

[18] M. Vijayagopal, P. Zanchetta, L. Empringham, L. de Lillo, L. Tarisciotti, and P. Wheeler, "Control of a direct matrix converter with modulated model-predictive control," *IEEE Trans. Ind. Appl.*, vol. 53, no. 3, pp. 2342–2349, May/Jun. 2017.

[19] M. Rivera, A. Wilson, C. A. Rojas, J. Rodriguez, J. R. Espinoza, P. W. Wheeler, and L. Empringham, "A comparative assessment of model predictive current control and space vector modulation in a direct matrix converter," *IEEE Trans. Ind. Electron.*, vol. 60, no. 2, pp. 578–588, Feb. 2013.

[20] H. M. Nguyen, H.-H. Lee, and T.-W. Chun, "Input power factor compensation algorithms using a new direct-SVM method for matrix converter," *IEEE Trans. Ind. Electron.*, vol. 58, no. 1, pp. 232–243, Jan. 2011.

[21] D. Xiao and M. F. Rahman, "Sensorless direct torque and flux controlled IPM synchronous machine fed by matrix converter over a wide speed range," *IEEE Trans. Ind. Informat.*, vol. 9, no. 4, pp. 1855–1867, Nov. 2013.

[22] K. You, D. Xiao, M. F. Rahman, and M. N. Uddin, "Applying reduced general direct space vector modulation approach of AC-AC matrix converter theory to achieve unity power factor controlled three-phase AC-DC matrix rectifier," in *Proc. IEEE Ind. Appl. Soc. Annu. Meeting*, Oct. 2011, pp. 1–7.

[23] H. W. van der Broeck, H.-C. Skudelny, and G. V. Stanke, "Analysis and realization of a pulsewidth modulator based on voltage space vectors," *IEEE Trans. Ind. Appl.*, vol. IA-24, no. 1, pp. 142–150, Jan. 1988.

[24] D. G. Holmes and T. A. Lipo, *Pulse Width Modulation for Power Converters: Principles and Practice*. Hoboken, NJ, USA: Wiley, 2003.

[25] K. Zhou and D. Wang, "Relationship between space-vector modulation and three-phase carrier-based PWM: A comprehensive analysis [three-phase inverters]," *IEEE Trans. Ind. Electron.*, vol. 49, no. 1, pp. 186–196, Feb. 2002.

[26] L. Huber and D. Borojevic, "Space vector modulated three-phase to three-phase matrix converter with input power factor correction," *IEEE Trans. Ind. Appl.*, vol. 31, no. 6, pp. 1234–1246, Nov. 1995.

[27] D. Casadei, G. Serra, and A. Tani, "Reduction of the input current harmonic content in matrix converters under input/output unbalance," *IEEE Trans. Ind. Electron.*, vol. 45, no. 3, pp. 401–411, Jun. 1998.

[28] C. Schauder and H. Mehta, "Vector analysis and control of advanced static VAr compensators," *IEE Proc. C, Gener., Transmiss. Distrib.*, vol. 140, no. 4, pp. 299–306, Jul. 1993.

[29] F. Gao and M. R. Iravani, "Dynamic model of a space vector modulated matrix converter," *IEEE Trans. Power Del.*, vol. 22, no. 3, pp. 1696–1705, Jul. 2007.

[30] C. Klumpner and F. Blaabjerg, *Fundamentals of the Matrix Converter Technology*. New York, NY, USA: Academic, 2002, ch. 3.

[31] T. Kume, K. Yamada, T. Higuchi, E. Yamamoto, H. Hara, T. Sawa, and M. M. Swamy, "Integrated filters and their combined effects in matrix converter," *IEEE Trans. Ind. Appl.*, vol. 43, no. 2, pp. 571–581, Mar. 2007.

[32] P. Cortes, S. Kouro, B. La Rocca, R. Vargas, J. Rodriguez, J. I. Leon, S. Vazquez, and L. G. Franquelo, "Guidelines for weighting factors design in model predictive control of power converters and drives," in *Proc. IEEE Int. Conf. Ind. Technol.*, Feb. 2009, pp. 1–7.
[33] Z. Malekjamshidi, M. Jafari, J. Zhu, and D. Xiao, "Bidirectional power flow control with stability analysis of the matrix converter for microgrid applications," *Int. J. Elect. Power Energy Syst.*, vol. 110, pp. 725–736, Sep. 2019.
[34] D. Casadei, G. Serra, A. Tani, A. Trentin, and L. Zarri, "Theoretical and experimental investigation on the stability of matrix converters," *IEEE Trans. Ind. Electron.*, vol. 52, no. 5, pp. 1409–1419, Oct. 2005.

ZAHRA MALEKJAMSHIDI (S'13–M'19) received the B.E. and M.E. degrees in electrical engineering from Shiraz University, Shiraz, Iran, in 1998 and 2001, respectively, and the Ph.D. degree from the University of Technology Sydney (UTS), Sydney, Australia, in 2018. From 2002 to 2012, she was a research engineer in industries and contributed to the design and development power electronic projects. Her current research interests include matrix converters, dc–dc converters, renewable energy technologies, and smart micro-grids.

MOHAMMAD JAFARI (M'12–SM'19) received the B.E. degree in electrical engineering from Shiraz University, Shiraz, Iran, in 1998, the M.E. degree in electrical engineering from Guilan University, Rasht, Iran, in 2001, and the Ph.D. degree in electrical engineering from the University of Technology Sydney (UTS), Sydney, Australia, in 2017. He has been contributed to the design and development of power electronics projects as a Research Engineer and Academician, since 2002. He has authored or coauthored more than 60 journals and peer-reviewed conference papers and two book chapters. His current research interests include power electronic converters, switching mode power supplies, renewable energy systems, and smart micro-grids.

JIANGUO ZHU (S'93–M'96–SM'03) received the B.E. degree from the Jiangsu Institute of Technology, Jiangsu, China, in 1982, the M.E. degree from the Shanghai University of Technology, Shanghai, China, in 1987, and the Ph.D. degree from the University of Technology Sydney (UTS), Sydney, Australia, in 1995, all in electrical engineering, where he was appointed as a Lecturer, in 1994, and promoted as a Full Professor, in 2004, and a Distinguished Professor of electrical engineering, in 2017. In 2018, he joined the University of Sydney, Australia, as a Full Professor, and the Head of the School of Electrical and Information Engineering. His research interests include computational electromagnetics, measurement and modeling of magnetic properties of materials, electrical machines and drives, power electronics, renewable energy systems, and smart micro grids.

DAN XIAO (M'06) received the bachelor's and master's degrees in electrical engineering from the Shenyang University of Technology, Shenyang, China, in 2001 and 2004, respectively, and the Ph.D. degree in electrical engineering from the University of New South Wales (UNSW Australia), Sydney, Australia, in 2010, where he is currently a Technical Support with the Energy System Research Laboratories. His research interests include sensorless control and online parameter estimation of ac machines, model predictive control for power converter and drives, matrix converters, and solid-state transformers.